Heisenberg-like ferromagnetism in 3d-4f intermetallic La_{0.75}Pr_{0.25}Co_{2}P_{2} with localized Co moments

P. Lampen, M. H. Phan, H. Srikanth, K. Kovnir, P. Chai, and M. Shatruk

Phys. Rev. B **90**, 174404 — Published 6 November 2014

DOI: 10.1103/PhysRevB.90.174404

Heisenberg-like ferromagnetism in 3*d*-4*f* intermetallic $La_{0.75}Pr_{0.25}Co_2P_2$ with localized Co moments

P. Lampen, M.H. Phan,* and H. Srikanth*

Department of Physics, University of South Florida, Tampa, FL 33620, USA

K. Kovnir,[a,b] P. Chai,[a] and M. Shatruk[a]

[a] *Department of Chemistry and Biochemistry, Florida State University, Tallahassee, FL 32306, USA*

[b] *Department of Chemistry, University of California, Davis, CA 95616, USA*

The critical behavior near the continuous paramagnetic to ferromagnetic transition in a single crystal of $La_{0.75}Pr_{0.25}Co_2P_2$ has been determined based on high-resolution bulk magnetization data near T_C ~167 K, where long-range order is established in the Co sublattice. Scaling equation of state analysis and the Kouvel-Fisher method under a moderate applied magnetic field yielded critical exponents ($\beta = 0.3685 \pm 0.0017$, $\gamma = 1.3361 \pm 0.0083$) consistent with the $d = 3$, $n = 3$ Heisenberg model of short-range interactions. Calculation of the Rhodes-Wohlfarth ratio confirmed that a localized rather than itinerant description of the 3*d* Co moments is appropriate in the ferromagnetic region of the sample. The critical susceptibility exponent γ was found to decrease systematically from the Heisenberg model value toward the mean-field model value as the maximum applied magnetic field considered in the analysis was increased above 2 T. The phenomenon is discussed in terms of mixed exchange mechanisms due to the coexistence of 3*d* and 4*f* magnetic sublattices and ordered clusters in the paramagnetic region.

PACS: 75.47.Lx, 75.30.Sg

Keywords: Laves phase compounds; Critical magnetic behavior; Magnetic anisotropy

*Corresponding authors: phanm@usf.edu and sharihar@usf.edu

I. INTRODUCTION

Intermetallic compounds combining rare-earth (R) and transition metal (T) elements continue to generate interest from both a technological perspective and one of fundamental physics.[1-4] Coexistence of localized 4f and itinerant 3d magnetic sublattices in such compounds provides an excellent framework to study competition between long-range RKKY and/or superexchange interactions and direct exchange.[1, 5] Among binary R_xT_y compounds, the Laves phases RT_2 are noteworthy for their exchange driven metamagnetism,[3, 6-8] while the strong effective 3d-4f coupling fields in R_2T_{17} materials produce large magnetocrystalline anisotropy while maintaining a high magnetic moment – a fact that has been exploited in permanent magnet applications.[9, 10] In ternary compounds the incorporation of a third element X (P, As, Si, Ge, B, etc.) provides an additional handle to manipulate electronic and structural parameters, thus influencing the magnetic properties of the R and T sublattices.[5, 11] The $ThCr_2Si_2$-type intermetallics crystallize in a relatively simple tetragonal structure, with alternating T_2X_2 and R layers stacked along the c-axis.[12] Nevertheless, these RT_2X_2 systems exhibit complex H-T phase diagrams, including incommensurate magnetic structures, Kondo lattices and quantum critical points (QCPs), re-entrant ferromagnetism, and metamagnetic transitions.[13-17]

The classification of the order of the magnetic transition in ferromagnetic RT_2X_2 systems has been of interest due to the potential application of these materials as low-temperature magnetic refrigerants.[18-20] Both first and second order paramagnetic to ferromagnetic transitions are observed,[4, 21-23] in some cases depending sensitively on the composition. While the determination of transition order is not uncommon, relatively few detailed investigations of the critical properties of ferromagnetic RT_2X_2 compounds are available in the literature.[24-26] In one

recent exception,[26] a study of the magnetism of $La_{1-x}Nd_xMn_2Si_2$ found mean-field-like critical exponents for the $x = 0.35$ composition.

The RT_2P_2 phosphide compounds manifest simpler magnetic properties than the ternary silicides and germanides (X = Si, Ge) and have been relatively less studied. With the exception of $LaCo_2P_2$ which undergoes a ferromagnetic transition at 132 K,[27] the other RCo_2P_2 phases are antiferromagnets.[28] However, a number of recent observations have elaborated on interesting effects in mixed and doped phosphide phases.[29-31] In particular, a variety of magnetic transitions were reported in solid solutions of $La_{1-x}Pr_xCo_2P_2$, despite the relatively simple magnetism of the end members of the series, $LaCo_2P_2$ and $PrCo_2P_2$.[27, 32] While the planar spacing in $LaCo_2P_2$ is anomalously large compared to the rest of the RCo_2P_2 series, the substitution of Pr for La decreases the interlayer separation and lengthens the Co-Co bonds, resulting in the enhancement of the T_C from 132 K for $x = 0$ to 170 K for $x = 0.25$.[27, 33]

While a quasi-2D character might be inferred from the stacked planes of magnetic ions in the $ThCr_2Si_2$ crystal structure, the well-established ferromagnetic and antiferromagnetic coupling between T_2X_2 layers along the c-axis suggests that a three dimensional magnetic description is appropriate. As in the RMn_2Ge_2[5] compounds a hierarchy of exchange couplings can be expected in RCo_2P_2: interlayer Co-Co, Co-R, and R-R, mediated through superexchange pathways or the RKKY interaction. Therefore the potential for magnetic inhomogeneity due to competing interactions exists. However, these mechanisms act as a perturbation of the direct exchange between co-planar Co atoms, which dominates the magnetism in the system. Due to the potential for delocalized magnetic moments in 3d subsystems, the question of the expected range of the interactions in the system is non-trivial. To address this point, we have performed a detailed analysis of the critical exponents of the paramagnetic to ferromagnetic transition in a single crystal of $La_{0.75}Pr_{0.25}Co_2P_2$. Our study shows that this intermetallic compound belongs to the 3D

Heisenberg class with short-range ferromagnetic interaction, and possesses a localized Co moment in the ferromagnetic region.

II. EXPERIMENTAL DETAILS

The preparation and characterization of $La_{0.75}Pr_{0.25}Co_2P_2$ single crystals have been reported in detail elsewhere.[27,32] In brief, high purity powders of lanthanum, praseodymium, red phosphorus, and cobalt were used along with tin shots in a tin flux synthetic procedure. In an argon-filled drybox, the materials were mixed according to the ratio La:Pr:Co:P:Sn = 1.6(1-*x*):1.6*x*:2:2:30 (*x* = 0.25), with total mass equal to 25 g, and sealed under vacuum in 20 mm inner diameter silica tubes. The mixtures were annealed at 1150 K for 10 days, then the tubes were removed from the furnace and allowed to cool to room temperature. The tin matrix was removed by soaking in dilute HCl, yielding large single crystals of up to 5 mm x 5 mm x 0.1 mm (Fig. 1a). The presence of any residual Sn was ruled out by magnetic measurements, which indicated a lack of any diamagnetic contribution associated with the superconducting transition in Sn at 3.72 K. The phase purity of the bulk products has been confirmed by powder X-ray diffraction while the elemental composition was confirmed by the energy-dispersive X-ray microanalysis as reported in our earlier work.[27, 32]

Magnetic measurements were carried out using a Quantum Design Physical Property Measurement System (PPMS) with a 7 T vibrating sample magnetometer (VSM) option and an ACMS option. Temperature dependent dc magnetization was measured between 5 K and 300 K, and temperature dependent ac susceptibility was measured between 40 K and 250 K. The *M* vs. *H* isotherms were measured in the range 160 K ≤ T ≤ 187 K. Isothermal magnetization versus magnetic field data around T_C were collected at 0.1 T increments up to 4.5 T, with a temperature interval of 0.25 K. To ensure temperature stabilization, a wait time of 10 minutes was imposed

after reaching the temperature set point and before recording each subsequent isotherm. The external applied magnetic field H_{ext} was corrected for demagnetizing effects to obtain the effective internal magnetic field $H_{eff} = H_{ext} - NM\,(T, H_{ext})$ in the sample. The demagnetization constant N was determined from the slope of the M (H) curves near zero field (± ~5 mT). The scaling analysis that follows below was performed using the effective values of magnetic field. AC susceptibility measurements were carried out in a driving field of $\mu_0 H_{ac}$ =1 mT and f = 5 kHz, taking care to demagnetize the sample environment before data collection to eliminate trapped fields.

III. THEORETICAL BACKGROUND

A. Critical exponents and universality

Due to the diverging correlation length of the critical fluctuations as a continuous phase transition point is approached, the microscopic details of a system become insignificant. Thus, diverse materials will show a universal behavior in the critical region. In principle, such universality classes depend only on the effective dimension of the lattice d and order parameter n, and possess a characteristic set of critical exponents that govern the scaling of relevant quantities near T_C.[34] The departure of a thermodynamic quantity from its $T = T_C$ value shows a power law dependence on temperature near a magnetic order-disorder phase transition. The spontaneous magnetization and initial susceptibility can be expressed as functions of the reduced temperature $\epsilon = (T - T_C)/T_C$ as follows:

$$M_S(T) = M_0(-\epsilon)^{\beta}, \qquad \epsilon < 0 \tag{1}$$

$$\chi_0^{-1}(T) = \Gamma(\epsilon)^{\gamma}, \qquad \epsilon > 0 \tag{2}$$

$$M = XH^{1/\delta}, \qquad \epsilon = 0 \tag{3}$$

where M_0, Γ, and X are the critical amplitudes.[35] Strictly, these expressions are valid only in a narrow range around T_C (i.e. $|\epsilon| \to 0$).

B. Scaling equations of state

Of the critical exponents defined above and those governing other thermodynamic quantities (e.g. heat capacity), only two are independent. The relationships among the various critical exponents can be written explicitly if one assumes the validity of the scaling hypothesis, that is, that the Gibbs potential is a generalized homogeneous function of H and ϵ.[36] In particular, the Widom scaling relation $\delta = 1 + \gamma/\beta$, is relevant to the discussion of the critical exponents of the paramagnetic-ferromagnetic transition as it allows the experimentally determined value of δ to be compared with the expected value based on β and γ obtained through independent analyses.

While there are several techniques that allow a more-or-less direct measurement of a critical exponent, e.g. neutron diffraction in the ordered region, the most common approach is based on analysis of bulk magnetization data and a magnetic equation of state. Scaling makes specific predictions concerning the form of the equation of state. In particular, scaling requires that there exist two parameters a and b such that

$$G\left(\lambda^a H, \lambda^b \epsilon\right) = \lambda G(H, \epsilon), \tag{4}$$

for any λ. Recalling that $M = -[\partial G(H,T)/\partial H]_T$, (4) can be manipulated through the choice of a, b, and λ to yield various formulations of a magnetic equation of state. Commonly used forms in the literature are [36, 37]

$$m = f_{\pm}(h) \tag{5}$$

$$H = M^{\delta} h(x) \tag{6}$$

$$h/m = \pm a_{\pm} + b_{\pm} m^2 \,, \tag{7}$$

where $m \equiv |\epsilon|^{-\beta} M(H, \square)$, $h \equiv |\epsilon|^{-\beta\delta} H$, and $x \equiv \epsilon M^{-1/\beta}$. In (5), the expression $f_{\pm}(h) = M(h, \epsilon/|\epsilon| = \pm 1)$ define two universal curves onto which the rescaled magnetization collapse above and below T_C, given a proper choice of β, γ, and T_C. While the collapse of data onto universal curves in this way can in principle be used to determine the correct critical exponents and amplitudes of a magnetic system, a more empirical approach is available using the Arrott-Noakes equation of state,

$$(H/M)^{1/\gamma} = A\epsilon + BM^{1/\beta} \,, \tag{8}$$

a special case of (5) and (6). In this case the proper choice of β and γ will cause the M (H,T) data to form a series of parallel straight lines in a plot of $M^{1/\beta}$ vs. $(H/M)^{1/\gamma}$, with the isotherm at $T = T_C$ passing through the origin. The zero-field quantities $M_S(T)$ and $\chi_0^{-1}(T)$ can thus be obtained by linear extrapolation to the ordinate and abscissa axes, respectively, and compared with (1) and (2). This approach leads to more reliable values of critical quantities as compared with other equations of state as it involves only two free parameters (β and γ: prior knowledge of T_C is not required).[37]

IV. RESULTS

A. Temperature dependence

The temperature-dependent magnetization of the $La_{0.75}Pr_{0.25}Co_2P_2$ single crystal is shown in Fig. 1 (c). This measurement was acquired under a field-cooled-warming (FCW) protocol. The magnetic interaction in the sample is highly anisotropic, as evidenced by the markedly different

behavior of the magnetization with a 10 mT DC magnetic field applied along the *c*-axis or in the *ab* plane. Early neutron diffraction work has established ferromagnetic intralayer Co-Co alignment in both $LaCo_2P_2$ and $PrCo_2P_2$.[28, 38] In $PrCo_2P_2$ the Co moments are oriented along the *c*-axis with antiferromagnetic interlayer coupling while in $LaCo_2P_2$ the Co moments lie in-plane with ferromagnetic alignment between the planes. In $La_{0.75}Pr_{0.25}Co_2P_2$ the Co sublattice is oriented in the *ab* plane in the temperature range $T_{C2} < T < T_C$,[32] and the easy direction of magnetization is in-plane (Fig. 1b). A reorientation of the easy axis was recently reported in this compound concurrent with the ordering of the Pr sublattice at $T_{C2} \sim 70$ K.[32] The result is antiparallel and nearly compensating Co and Pr sublattices pointing along the *c*-axis, causing the net magnetization to drop almost to zero below T_{C2}. Above T_{C2}, there is no long-range order of Pr moments, and the magnetic properties of the system are dominated by the ordered Co sublattice. No significant hysteresis is observed between field-cooled and zero-field-cooled thermomagnetic curves (not shown).

Temperature-dependent susceptibility data measured with a low-amplitude AC field show a sharp transition that becomes demagnetization-limited below T_C (Fig. 1d). The Curie temperature is estimated to be near 166 K by determining the kink-point in the susceptibility. Above T_C, inverse susceptibility $\chi^{-1}(T)$ curves are linear up to high temperatures, in agreement with the Curie-Weiss law. The paramagnetic moment per alloy atom p_{eff} in Bohr magnetons is given by $p_{eff} \cong 2.83(d\chi^{-1}/dT)^{-1/2}$, where $\chi(T)$ is the molar susceptibility. The quantity p_{eff} was determined for the susceptibility measured under magnetic fields of 1 T, 2 T, 3 T, 4 T, and 5 T. The effective moment in a paramagnetic material is often independent of the applied field. However, we found that a minimum occurred in p_{eff} at 2 T followed by a slow increase for higher fields. We revisit this observation in the discussion section.

B. Determination of the critical exponents

To determine the critical exponents in the system using the Arrott-Noakes equation of state for analysis, closely-spaced M (H) curves were acquired in the critical region of $La_{0.75}Pr_{0.25}Co_2P_2$. These data were then re-scaled according to (8) for various choices of β and γ. In systems with a long-range ferromagnetic interaction, a mean field description of critical behavior is appropriate ($\beta = 0.5$, $\gamma = 1.0$), and $M^{1/\beta}$ vs. $(H/M)^{1/\gamma}$ is simply the well-known Arrott plot. From Fig. 2(a) it can be seen that for $La_{0.75}Pr_{0.25}Co_2P_2$, the isotherms constructed in this way deviate from linearity across the range of fields used (0.1 T < $\mu_0 H$ < 2.0 T). In some cases reliable results can still be obtained for disordered ferromagnets using Arrott plots through quadratic extrapolation to the zero-field values.[36] We found that this did not describe our data well away from T_C, but a parabolic fit to the 166.5 K isotherm was successful and passed through the origin, indicating that the critical isotherm is at ~166.5 K, in agreement with Fig. 1.

The Heisenberg model is a natural choice to describe a ferromagnet with short-range interactions, as it considers localized moments on a regular lattice with only nearest-neighbor interactions. Unlike the mean-field model, an exact solution for the critical exponents of the 3D-Heisenberg model is not available, but a number of computational and theoretical techniques have been applied, which consistently yield estimates near $\beta \sim 0.37$, $\gamma \sim 1.33$.[39] From Fig. 2(b) it is clear that the Heisenberg exponents are much more successful in creating parallel linear isotherms in the modified Arrott plot. The $M_S(T)$ and $\chi_0^{-1}(T)$ curves obtained from linear extrapolation of the data in 2(b) are shown in Fig. 3 and well-fit to the power law dependences given in (1) and (2).

If interactions not accounted for in the theory of critical phenomena influence the magnetization or if the range over which an exponent is calculated is far away from the critical temperature, effective rather than asymptotic exponents result from the scaling equation of state analysis. The effective critical exponents of a system are given by $\beta_{eff}(\epsilon) = \partial[\ln M_S(\epsilon)]/\partial(\ln \epsilon)$ and $\gamma_{eff}(\epsilon) = \partial\left[\ln \chi_0^{-1}(\epsilon)\right]/\partial(\ln \epsilon)$ and are related to the asymptotic exponents in such a way that the effective exponents approach the asymptotic ones as $\epsilon \to 0$.[35, 40] In general, for crystalline ferromagnets, $\gamma_{eff}(\epsilon)$ decreases monotonically at large ϵ outside the critical region toward the mean-field value ($\gamma = 1$), while in amorphous ferromagnets a peak in $\gamma_{eff}(\epsilon)$ before the decrease at large ϵ is a well-documented phenomenon.[37, 41] The range of ϵ for which β_{eff} and γ_{eff} remain near a constant value is referred to as the asymptotic critical region (ACR). Discrepancies in reported critical exponents for similar or identical systems are most often the result of a range of analysis that is too wide. The effective exponents of $La_{0.75}Pr_{0.25}Co_2P_2$ are shown in Fig. 4. In the temperature range considered, the effective exponents remain constant within error near their 3D Heisenberg values (dashed lines in Fig. 4), indicating that the ACR extends beyond ~1.12 T_C. The error in Fig. 4 and in subsequent analysis is determined by differential propagation of the uncertainty in relevant fitted quantities.

Within the ACR, the most reliable method for obtaining the exact values of the critical exponents based on modified Arrott plots is the iterative Kouvel-Fisher method. Equations (1) and (2) can be re-written in the form

$$M_S(T)[\mathrm{d}M_S(T)/\mathrm{d}T]^{-1} = (T - T_C)/\beta \tag{9}$$

$$\chi_0^{-1}(T)\left[\mathrm{d}\chi_0^{-1}(T)/\mathrm{d}T\right]^{-1} = (T - T_C)/\gamma. \tag{10}$$

Thus, plots of $M_S(T)\left[dM_S(T)/dT\right]^{-1}$ vs. T and $\chi_0^{-1}(T)\left[d\chi_0^{-1}(T)/dT\right]^{-1}$ vs. T result in straight lines with slopes of $1/\beta$ and $1/\gamma$ respectively, which intercept the temperature axis at T_C (Fig. 5). The values of β, γ, and T_C obtained in this way are used to construct a new Arrott-Noakes plot, and the process is repeated until the desired convergence in the critical values is achieved. This procedure was carried out in the range $-0.05 < \epsilon < 0.05$, with rapid convergence of the critical exponents to $\beta = 0.369 \pm 0.002$ and $\gamma = 1.336 \pm 0.008$ with $T_C = 166.8 \pm 0.9$.

Although the assumption of scaling is implicit in the above analysis, the possibility of systematic errors introduced by extrapolation exists and thus additional confirmation is usually made of the validity of other scaling equations of state and the relationship between the exponents. A log-log plot of field-dependent magnetization is shown in Fig. 6 at temperatures in the vicinity of T_C. According to (3), the exponent δ can be determined from the inverse slope of the critical isotherm. A linear fit of the $T = 166.75$ K isotherm results in $\delta = 4.68$, close to the value expected from the Widom relation of $\delta = 1 + \gamma/\beta = 4.63$ based on the results of the Kouvel-Fisher technique. The scaling exponent governing the peak magnetic entropy change $\Delta S_M^{pk} \propto H^n$ is also related to the magnetization and susceptibility exponents as $n = 1 + (\beta - 1)/(\beta + \gamma)$.[42] The magnetic entropy change in the system (Fig. 7, inset) was calculated by integration between successive isotherms according to the thermodynamic Maxwell relation.[42] Using the Kouvel-Fisher-generated values of β and γ, we can expect that $n = 0.63$. Re-scaling the field axis to produce a plot of ΔS_M^{pk} vs. H^n with $n = 0.63$ reveals the expected linear relationship (Fig. 7), confirming correctness of the exponent.

From Fig. 8(a) it can be seen that the magnetization data satisfy scaling equation of state (5) [$m = f_{\pm}(h)$] by collapsing onto two universal curves f_- and f_+ below and above T_C. However,

due to the insensitive nature of the log-log scale, the same quality of collapse is achievable with many sets of parameter values – typically varying between ±2% of the true T_C and ±10% of the true β and γ.[43, 44] On the other hand, equation of state (7) [$h/m = \pm a_{\pm} + b_{\pm}m^2$] is considerably more sensitive to deviations from the asymptotic critical values, and the data also show good collapse when re-scaled in this way (Fig. 8b). However, we note that in this case there also exists a small range of parameter values that will yield similar results –a direct consequence of three free parameters in (5) and (7) as opposed to two in the Arrott-Noakes approach.

C. Magnetic field dependence of the critical properties

While much is known regarding the temperature dependence of critical exponents, the influence of magnetic field on critical behaviors in ferromagnetic materials is not often discussed.[45, 46] $La_{0.75}Pr_{0.25}Co_2P_2$ shows relatively soft ferromagnetic behavior below T_C, and is saturated by an applied field of 2 T. As such, the critical exponents above this field should in principle remain independent of the magnetic field applied. However, we observed an anomalous behavior when our analysis was extended to higher magnetic fields. As illustrated in Fig. 9(a), the maximum magnetic field was increased incrementally from 2.0 T to 4.5 T, and the Kouvel-Fisher process described above was repeated for 0.1 T < $\mu_0 H$ < $\mu_0 H_{MAX}$. The results (Fig. 9 b-c) show that β remains near the 3D Heisenberg value, but slowly increases above ~3 T while the decrease in γ is large and systematic as the maximum magnetic field is increased.

V. DISCUSSION

The description of magnetic properties in metallic systems has historically been approached from two extremes – band theoretical models in which itinerant magnetism arises as the result of the spin splitting of conduction electron bands, or the localized Heisenberg model in

which coupled neighboring moments fluctuate in orientation but not in magnitude. These models can be regarded as limiting cases, strictly applicable, respectively, to paramagnetic metals far from the ferromagnetic instability and ferromagnetic metals with nearly saturated or stable atomic spin polarizations.[47, 48] Many 3*d* transition metal compounds fall in an intermediate range between localized and fully itinerant systems, with correlated motions (spin fluctuations) among well-defined local moments, and theoretical models of both types have been successful in describing experimental results.[49, 50] While the nature of the magnetism of a 3*d* subsystem in RT_2X_2 intermetallics is unclear at the present time [see Ref. 5 and references therein], the Stoner criterion – based on band structure calculations of the density of states at the Fermi level – has been successful in predicting the appearance of ferromagnetism and itinerant electron metamagnetism in a number of such systems. Recent electronic structure calculations show that the ferromagnetism in $LaCo_2P_2$ and $La_{0.88}Pr_{0.12}Co_2P_2$ can be explained by the fulfillment of the Stoner criterion.[27] Generally, itinerant magnets belong to classical or mean-field universality classes (long-range spin-spin interaction).[51, 52] Nevertheless, the conformity of the critical properties determined for $La_{0.75}Pr_{0.25}Co_2P_2$ to the isotropic $d = 3$ $n = 3$ Heisenberg exchange of the form $J(r) \sim e^{(-r/b)}$ is consistent with stable localized Co moments.

To confirm this finding, we evaluate the Rhodes-Wohlfarth ratio in $La_{0.75}Pr_{0.25}Co_2P_2$. The Rhodes-Wohlfarth ratio compares the number of carriers per magnetic atom (q_p) derived from the Curie-Weiss constant to q_s, the spontaneous moment below T_C. In saturated ferromagnets, these quantities are equal, while in weak itinerant ferromagnets it is typical that $q_p/q_s \gg 1$.[35] In the paramagnetic region q_p is related to the total effective moment as $p_{eff} = \sqrt{q_p\left(q_p + 2\right)}$. Usually, q_s is taken to be the moment per magnetic alloy atom at low temperature ($T \rightarrow 0$).

However, as $La_{0.75}Pr_{0.25}Co_2P_2$ is a ferrimagnet below ~ 70 K with nearly zero net magnetization, we adopt the approach of Pramanik et al. in determining q_s well below T_C but within the ferromagnetic temperature range.[35] At 100 K, the M (H) curve (not shown) saturates at 0.76 $\mu_B/f.u.$ As the Pr subsystem shows no long range order at this temperature,[32] the magnetization may be assigned to the Co atoms, i.e. $q_s = 0.38\,\mu_B/\text{Co}$. This result is in good agreement with the Co moment determined by us earlier via neutron diffraction.[32] Above T_C, both Pr and Co contribute to the total effective moment as $p_{eff}^2 = 0.25(p_{Pr})^2 + 2(p_{Co})^2$. To make a meaningful comparison to the ferromagnetic region, we account for the contribution of the Pr moments to the total p_{eff} by assuming the experimentally determined value of $3.12\,\mu_B$/Pr. [32] In this way we calculate the itinerancy of the Co moments.

The resulting Rhodes-Wohlfarth ratios are given in Fig. 10 for several values of magnetic field ranging from 1 T to 5 T. The shift of the effective paramagnetic moment noted above influences the value of q_p/q_s as the field is varied. However, the ratio remains close to 1 overall, confirming the dominant localized magnetic interaction indicated by the Heisenberg critical exponents. On the other hand, the parent compound $LaCo_2P_2$ has a slightly itinerant character ($q_p/q_s = 1.72$).[28] The doping of Pr^{3+} ($> 3\mu_B$) on the non-magnetic La^{3+} site is responsible for the observed change in the nature of the interaction in $La_{0.75}Pr_{0.25}Co_2P_2$. In addition to the applied external field, Pr ions experience an exchange field due to the surrounding Co ions given by $H_{ex} = -zA_{\text{Pr-Co}}m_{\text{Co}}/2{\mu_B}^2$, where z is the number of Co neighbors, m_{Co} is the magnetic moment per Co, and $A_{\text{Pr-Co}}$ is the coupling parameter between Pr and Co.[9] The effective molecular field associated with 3*d*-4*f* coupling favors antiparallel (parallel) alignment between the moments of Co and heavy (light) rare-earth elements in the RCo_2 series. In contrast to this trend, the

exchange interaction between the Co and light rare-earth (Pr) moments in $La_{0.75}Pr_{0.25}Co_2P_2$ is antiferromagnetic.[32]

The role of the 3*d*-4*f* exchange is important in understanding our observations in the paramagnetic region of $La_{0.75}Pr_{0.25}Co_2P_2$. As a paramagnetic 3*d*-4*f* compound acquires small net magnetization under the influence of an external applied field, the strong internal exchange fields between the 3*d* and 4*f* sublattices (> 100 T in some R_mCo_n compounds) can induce locally ordered regions in the form of small clusters (~7-8 Å) above T_C.[8] Clusters with an average antiparallel arrangement between 3*d* and 4*f* moments have been well-documented in RCo_2 compounds where *R* is a heavy rare earth element.[8, 53, 54] Opposing net paramagnetic magnetizations in the Pr and Co sublattices of $La_{0.75}Pr_{0.25}Co_2P_2$ are consistent with the observation of q_p/q_s values somewhat less than unity in Fig. 10. Such an arrangement partially cancels the magnetization, bringing the total susceptibility of the system below the expected value for free ion moments. In this scenario the dependence of the Rhodes-Wohlfarth ratio on the applied field reflects the evolution of ordered clusters. A small applied field is necessary to impart net (opposing) directions to the sublattices, but a moderate-to-large magnetic field ($\leq$ 5 T in $ErCo_2$)[8] will reverse the antiparallel sublattice, destroying the quasi-ferrimagnetic order. The minimum in q_p/q_s at ~ 2 T suggests a critical field above which the suppression of the clusters takes place.

To confirm the presence of ordered spin clusters above T_C, radio-frequency transverse susceptibility (TS) measurements were performed using a sensitive self-resonant tunnel diode oscillator. The details of the experimental setup and analysis of TS results have been reported elsewhere.[55, 56] In brief, peaks in the quantity $\Delta\chi_T/\chi_T$ % are theoretically predicted to occur at the anisotropy fields ($H_{dc} = \pm H_K$) and switching field ($H_{dc} = H_S$) of a material during a unipolar

sweep of the dc magnetic field. From Fig. 11(a) a double peak feature at $\pm H_K$ characteristic of a ferromagnetic material is observed in the TS scan of $La_{0.75}Pr_{0.25}Co_2P_2$ at 100 K (below T_C) as the dc magnetic field is swept from positive to negative saturation. Above T_C the maximum $\Delta\chi_T/\chi_T$ % drops precipitously, but significantly the double peak characteristic persists at 180 K (Fig. 11b), with H_K decreasing from ~500 Oe ($T < T_C$) to ~ 50 Oe. The presence of anisotropy peaks in this temperature range indicates weak ferromagnetic correlations (due to the presence of ferromagnetic clusters) in the paramagnetic region. A similar observation has also been reported for the case of $Pr_{0.5}Sr_{0.5}CoO_3$.[57]

Finally, we consider the field-dependence of the critical exponents. From Fig. 9 it can be seen that the susceptibility exponent is systematically depressed as fields above 2 T are considered, ranging between $\gamma = 1.34$ and $\gamma = 1.19$. In a magnetic system governed by various competing couplings, intrinsic systematic trends or crossover phenomena in the critical properties are possible.[57] In particular, the coexistence of long- and short-range interactions is known to cause a shift in the critical exponents away from the isotropic short range Heisenberg exponents and toward the mean-field values ($\beta = 0.5$ and $\gamma = 1$) as in the case of the elemental transition metals Fe and Ni.[44, 58] Such a shift manifests the simultaneous presence of Heisenberg exchange, $J(r) \sim e^{(-r/b)}$, and isotropic long-range exchange interactions of the form $J(r) \sim -J_\infty / r^{d+\sigma}$, $0 < \sigma < 2$, which render the Heisenberg fixed point unstable. From Fig. 9(b-c) the increase in β and decrease in γ with field are consistent with an increasing realization of long-range interactions as the strength of the external field grows. We consider this phenomenon in terms of the competing fields in the system: H_a, the external applied field, H_{ex}, the exchange field between Co and Pr, and $H_{Co\text{-}Co}$, the internal interaction field of the Co sublattice. While the tendency towards internal alignment of Co ions is the strongest interaction in the system, $H_{Co\text{-}Co}$ does not favor a particular direction, and so the orientation of the Co sublattice is determined by

the influence of H_a and H_{ex}. At low temperatures the antiferromagnetic H_{ex} dominates and the Co and Pr subsytems are anti-aligned. At higher temperatures the Pr magnetization is small and paramagnetic, so that the Co moments follow H_a (subject to the magnetocrystalline anisotropy) and the Pr moments experience competing tendencies to align with H_a (parallel to Co) and with H_{ex} (antiparallel to Co). With increasing external applied field the influence of H_{ex} becomes less significant, reducing the inhomogeniety in the exchange interactions acting on the Co system and increasing long-range ferromagnetic order. Above T_C this is equivalent to a suppression of the magnetic clusters with increasing field.

VI. CONCLUSIONS

In summary a Kouvel-Fisher method was used to determine the critical exponents of the ferromagnetic transition in the Co-sublattice of $La_{0.75}Pr_{0.25}Co_2P_2$, a 3*d*-4*f* intermetallic compound. Despite the itinerant nature of the parent compound $LaCo_2P_2$, the critical properties in the Pr-substituted compound were found to conform to the 3D Heisenberg model of isotropic short-range interactions due to competition between the applied field and the exchange field H_{ex} between 3*d* and 4*f* moments. The calculation of the Rhodes-Wohlfarth ratio confirmed a localized Co moment below $T_C \sim 167$ K. However, magnetic field was found to influence both the Rhodes-Wohlfarth ratio and the critical exponents. It is proposed that q_p is influenced by ordered antiparallel clusters in the paramagnetic region. As the external applied magnetic field is increased, a more homogeneous magnetic state is achieved in $La_{0.75}Pr_{0.25}Co_2P_2$ resulting in a shift in the critical exponents toward the mean-field model values as the Kouvel-Fisher procedure was repeated for increasingly large magnetic fields.

ACKNOWLEDGEMENTS

Research at USF (magnetic measurements and analysis) was supported by the U.S. Department of Energy, Office of Basic Energy Sciences, Division of Materials Sciences and Engineering under Award # DE-FG02-07ER46438.

References

1. R. J. Radwanski, Physica Stat. Sol. B **137**, 487-493 (1986).
2. M. D. Kuz'min and A. M. Tishin, in *Handbook of Magnetic Materials*, edited by K. H. J. Buschow (North-Holland, Amsterdam, 2008), Vol. 17.
3. N. K. Singh, K. G. Suresh, A. K. Nigam, S. K. Malik, A. A. Coelho and S. Gama, J. Magn. Magn. Mater. **317**, 68-79 (2007).
4. J. L. Wang, L. Caron, S. J. Campbell, S. J. Kennedy, M. Hofmann, Z. X. Cheng, M. F. M. Din, A. J. Studer, E. Bruck and S. X. Dou, Phys. Rev. Lett. **110**, 239901 (2013).
5. N. P. Kolmakova, A. A. Sidorenko and R. Z. Levitin, Low Temp. Phys. **28**, 653-668 (2002).
6. R. M. Moon, W. C. Koehler and J. Farrell, J. Appl. Phys. **36**, 978 (1965).
7. Y. G. Xiao, Q. Huang, Z. W. Ouyang, F. W. Wang, J. W. Lynn, J. K. Liang and G. H. Rao, Phys. Rev. B **73**, 064413 (2006).
8. J. Herrero-Albillos, F. Bartolome, L. M. Garcia, A. T. Young, T. Funk, J. Campo and G. J. Cuello, Phys. Rev. B **76**, 094409 (2007).
9. J. J. M. Franse, F. E. Kayzel and N. P. Thuy, J. Magn. Magn. Mater. **129**, 26-38 (1994).
10. S. D. Mao, M. S. Yan, X. Nie, K. Q. Sun, J. J. Jiang and Z. L. Song, J. Appl. Phys. **115**, 043912 (2014).
11. A. Szytula, Materials Science-Poland **24**, 737-751 (2006).
12. Z. Ban and M. Sikirica, Acta Crystallographica **18**, 594 (1965).
13. L. W. Li, G. H. Hu, I. Umehara, D. X. Huo, T. Namiki and K. Nishimura, J. Phys. Soc. Jpn. **81**, 073701 (2012).

14. G. Liang, R. Barber, Y. J. Tang, M. Croft, J. L. Cobb and J. T. Markert, Phys. Rev. B **51**, 214-222 (1995).

15. J. E. McCarthy, J. A. Duffy, C. Detlefs, M. J. Cooper and P. C. Canfield, Phys. Rev. B **62**, R6073-R6076 (2000).

16. O. Stockert and F. Steglich, Annu. Rev. Cond. Mat. Phys. **2**, 79-99 (2011).

17. Y. Tabata, T. Yamazaki, M. Okue, H. Nakamura and M. Matsuura, J. Phys.: Conf. Series **145**, 012078 (2009).

18. M. F. M. Din, J. L. Wang, S. J. Campbell, A. J. Studer, M. Avdeev, S. J. Kennedy, Q. F. Gu, R. Zeng and S. X. Dou, Appl. Phys. Lett. **104** (2014).

19. T. B. Zhang, Y. G. Chen, Y. B. Tang, E. Y. Zhang and M. J. Tu, Phys. Lett. A **354**, 462-465 (2006).

20. R. Zeng, S. X. Dou, J. L. Wang and S. J. Campbell, J. Alloys Compd. **509**, L119-L123 (2011).

21. J. L. Wang, S. J. Campbell, J. M. Cadogan, A. J. Studer, R. Zeng and S. X. Dou, Appl. Phys. Lett. **98**, 232509 (2011).

22. Y. Q. Chen, J. Luo, J. K. Liang, J. B. Li and G. H. Rao, J. Alloys Compd. **489**, 13-19 (2010).

23. J. L. Wang, S. J. Campbell, R. Zeng, C. K. Poh, S. X. Dou and S. J. Kennedy, J. Appl. Phys. **105** (2009).

24. J. H. Yang, B. Chen, H. D. Wang, Q. H. Mao, M. Imai, K. Yoshimura and M. H. Fang, Phys. Rev. B **88** (2013).

25. V. H. Tran and Z. Bukowski, J. Phys.: Condens. Matter **26**, 255602 (2014).

26. B. Emre, I. Dincer, Y. Elerman and S. Aksoy, Solid Stat. Sci. **22**, 1-7 (2013).

27. K. Kovnir, C. M. Thompson, H. D. Zhou, C. R. Wiebe and M. Shatruk, Chem. Mater. **22**, 1704-1713 (2010).

28. M. Reehuis, C. Ritter, R. Ballou and W. Jeitschko, J. Magn. Magn. Mater. **138**, 85-93 (1994).

29. S. A. Jia and R. J. Cava, Phys. Rev. B **82**, 180410 (2010).

30. K. Kovnir, V. O. Garlea, C. M. Thompson, H. D. Zhou, W. M. Reiff, A. Ozarowski and M. Shatruk, Inorg. Chem. **50**, 10274-10283 (2011).

31. K. Kovnir, W. M. Reiff, A. P. Menushenkov, A. A. Yaroslavtsev, R. V. Chernikov and M. Shatruk, Chem. Mater. **23**, 3021-3024 (2011).

32. K. Kovnir, C. M. Thompson, V. O. Garlea, D. Haskel, A. A. Polyanskii, H. D. Zhou and M. Shatruk, Phys. Rev. B **88**, 104429 (2013).

33. C. M. Thompson, A. A. Arico, K. Kovnir and M. Shatruk, J. Appl. Phys. **107**, 09E316 (2010).

34. H. E. Stanley, Rev. Mod. Phys. **71**, S358-S366 (1999).

35. A. K. Pramanik and A. Banerjee, Phys. Rev. B **79**, 214426 (2009).

36. S. N. Kaul, J. Magn. Magn. Mater. **53**, 5-53 (1985).

37. S. N. Kaul, IEEE Trans. Magn. **20**, 1290-1295 (1984).

38. M. Reehuis, P. J. Brown, W. Jeitschko, M. H. Moller and T. Vomhof, J. Phys. Chem. Solids **54**, 469-475 (1993).

39. M. Campostrini, M. Hasenbusch, A. Pelissetto, P. Rossi and E. Vicari, Phys. Rev. B **65**, 144520 (2002).

40. S. Srinath, S. N. Kaul and M. K. Sostarich, Phys. Rev. B **62**, 11649-11660 (2000).

41. A. Perumal, V. Srinivas, V. V. Rao and R. A. Dunlap, Phys. Rev. Lett. **91**, 137202 (2003).

42. V. Franco, A. Conde, J. M. Romero-Enrique and J. S. Blazquez, J. Phys.: Condens. Matter **20**, 285207 (2008).

43. P. D. Babu and S. N. Kaul, J. Phys.: Condens. Matter **9**, 7189-7222 (1997).

44. S. F. Fischer, S. N. Kaul and H. Kronmuller, Phys. Rev. B **65**, 064443 (2002).

45. P. Zhang, P. Lampen, T. L. Phan, S. C. Yu, T. D. Thanh, N. H. Dan, V. D. Lam, H. Srikanth and M. H. Phan, J. Magn. Magn. Mater. **348**, 146-153 (2013).

46. P. Sarkar, P. Mandal, A. K. Bera, S. M. Yusuf, L. S. S. Chandra and V. Ganesan, Phys. Rev. B **78**, 012415 (2008).

47. Y. Takahashi, *Spin fluctuation theory of itinerant electron magnetism*. (Springer-Verlag Berlin Heidelberg, 2013).

48. G. G. Lonzarich and L. Taillefer, J. Phys. C: Solid Stat. Phys. **18**, 4339-4371 (1985).

49. P. J. Jensen, K. H. Bennemann, P. Poulopoulos, M. Farle, F. Wilhelm and K. Baberschke, Phys. Rev. B **60**, 14994-14997 (1999).

50. J. H. Wu, T. Herrmann, M. Potthoff and W. Nolting, J. Phys.: Condens. Matter **12**, 2847-2855 (2000).

51. D. Belitz, T. R. Kirkpatrick and J. Rollbuhler, Phys. Rev. Lett. **94**, 247205 (2005).

52. A. Bhattacharyya, D. Jain, V. Ganesan, S. Giri and S. Majumdar, Phys. Rev. B **84**, 184414 (2011).

53. D. Gignoux and F. Givord, J. Phys. F: Met. Phys. **9**, 1409 (1979).

54. D. Gignoux, F. Givord and W. C. Koehler, Physica B & C **165**, 86-88 (1977).

55. N. A. F. Huls, N. S. Bingham, M. H. Phan, H. Srikanth, D. D. Stauffer and C. Leighton, Phys. Rev. B **83**, 024406 (2011).

56. S. Chandra, A. I. Figueroa, B. Ghosh, A. K. Raychaudhuri, M. H. Phan, P. Mukherjee and H. Srikanth, Physica B-Condensed Matter **407**, 175-178 (2012).

57. B. Padmanabhan, H. L. Bhat, S. Elizabeth, S. Rossler, U. K. Rossler, K. Dorr and K. H. Muller, Phys. Rev. B **75**, 024419 (2007).

58. J. Lago, M. J. Rosseinsky, S. J. Blundell, P. D. Battle, M. Diaz, I. Uriarte and T. Rojo, Phys. Rev. B **83**, 104404 (2011).

Figure captions

Fig. 1 (a) Image of $La_{0.75}Pr_{0.25}Co_2P_2$ single crystal. (b) Illustration of the $ThCr_2Si_2$-type unit cell of $La_{0.75}Pr_{0.25}Co_2P_2$ from Ref. 33. (c) Temperature dependent magnetization measured in a field-cooled-warming protocol under a 10 mT dc field applied parallel and perpendicular to the *c*-axis of a single crystal. (d) $\chi(T)$ with $H \| c$ under 1 mT amplitude ac magnetic field (left) and $\chi^{-1}(T)$ with a dc bias of 1 T (right).

Fig. 2 (a) Arrott plot of magnetization isotherms taken between 160 K and 187 K with $\Delta T = 0.25$ K. The line indicates the parabolic fit to the isotherm at 166.5 K. (b) Modified Arrott plot using 3D Heisenberg critical exponents. The line represents a linear fit to the isotherm at 166.75 K.

Fig. 3 Temperature dependence of M_S and χ_0^{-1} obtained from linear extrapolation of the data in Fig. 2(b). Lines represent best fits to equations (1) and (2).

Fig. 4 Effective exponents γ_{eff} and β_{eff} calculated as described in the text over the range of temperatures under consideration. Dashed lines are placed at the 3D Heisenberg model predictions for the respective exponents ($\gamma = 1.336$, $\beta = 0.368$).

Fig. 5 Kouvel-Fisher plots of magnetization data in the range -0.05 < □ < 0.05. Straight lines are linear fits to the data, from which β, γ, T_C^-, and T_C^+ are computed. The final value of T_C is taken as the average of T_C^- and T_C^+.

Fig. 6 ln M vs. ln $\mu_0 H$ for temperatures near the critical isotherm. δ is determined from the slope of the linear fit of the isotherm at 166.75 K according to equation (3).

Fig. 7 Peak magnetic entropy change versus H^n, where n = 0.63 is the prediction of the scaling relation combined with the results of the Kouvel-Fisher method.

Fig. 8 Re-scaling of the magnetization isotherms according to equations of state given in (a) Eqn. 5 and (b) Eqn. 7.

Fig. 9 (a) Illustration of the range of magnetic field under consideration in the Kouvel-Fisher analysis. Dependence of (a) γ and (b) β on the maximum magnetic field.

Fig. 10 Rhodes-Wohlfarth ratio (q_p/q_s) versus applied magnetic field.

Fig. 11 Unipolar transverse susceptibility scans at (a) 100 K and (b) 180 K.

Fig. 1

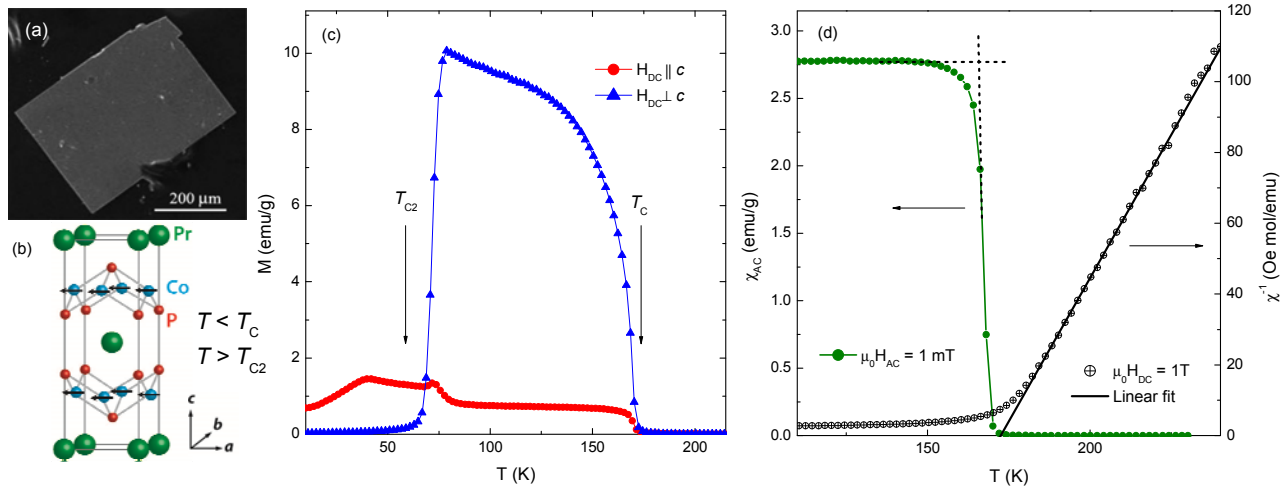
(a)
200 µm
(b)
Pr
Co
P
T < T_C
T > T_C2
c
b
a
(c)
H_DC ∥ c
H_DC ⊥ c
T_C2
T_C
M (emu/g)
T (K)
(d)
μ0H_AC = 1 mT
μ0H_DC = 1T
Linear fit
χ_AC (emu/g)
χ^-1 (Oe mol/emu)
T (K)

Fig. 2

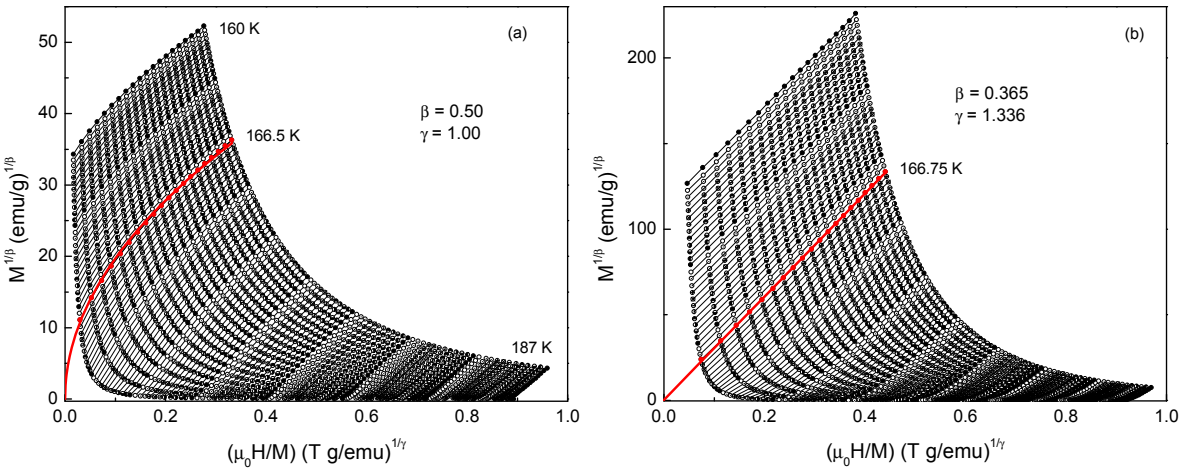
(a)
160 K
166.5 K
187 K
β = 0.50
γ = 1.00
M^1/β (emu/g)^1/β
(μ0H/M) (T g/emu)^1/γ
(b)
166.75 K
β = 0.365
γ = 1.336
M^1/β (emu/g)^1/β
(μ0H/M) (T g/emu)^1/γ

Fig. 3

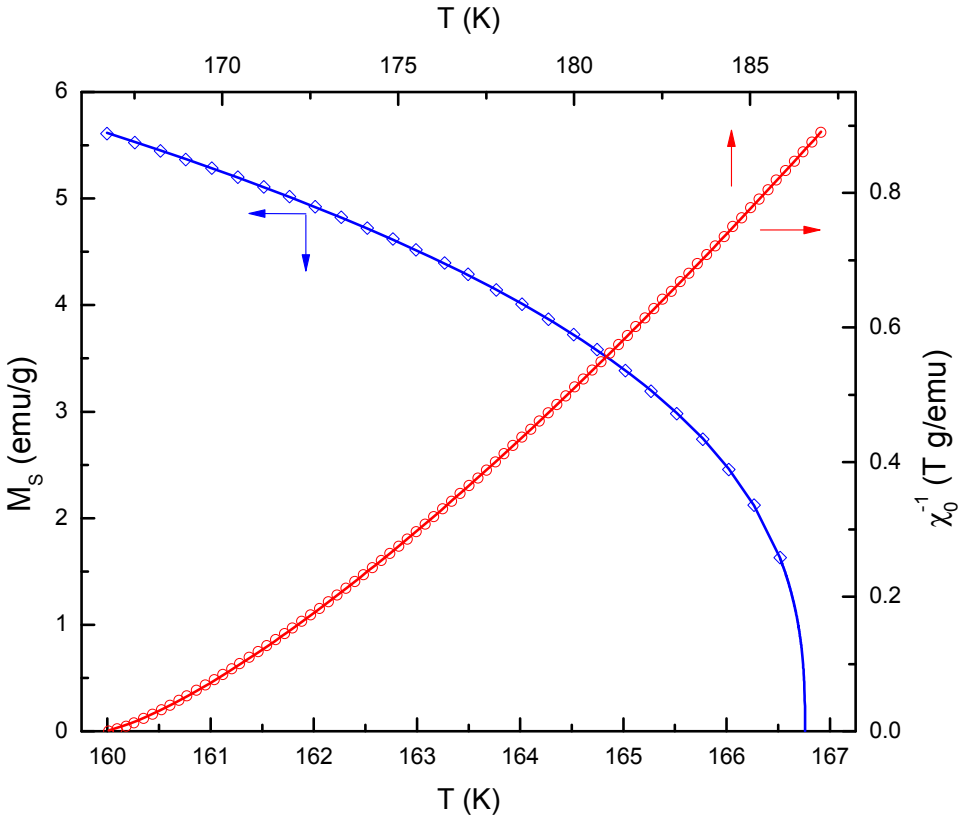
T (K)
170
175
180
185
6
5
4
3
2
1
0
M_S (emu/g)
0.8
0.6
0.4
0.2
0.0
χ_0^{-1} (T g/emu)
160
161
162
163
164
165
166
167
T (K)

Fig. 4

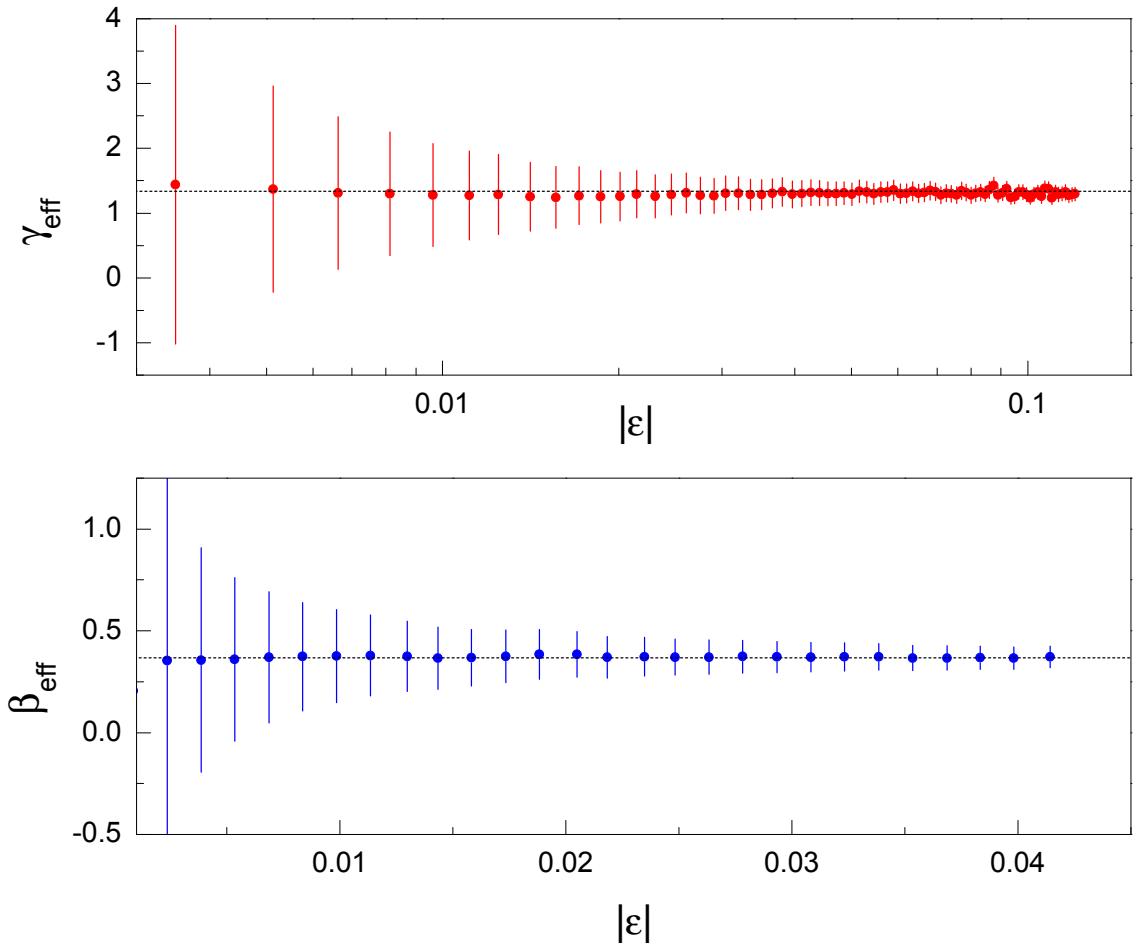

Fig. 5

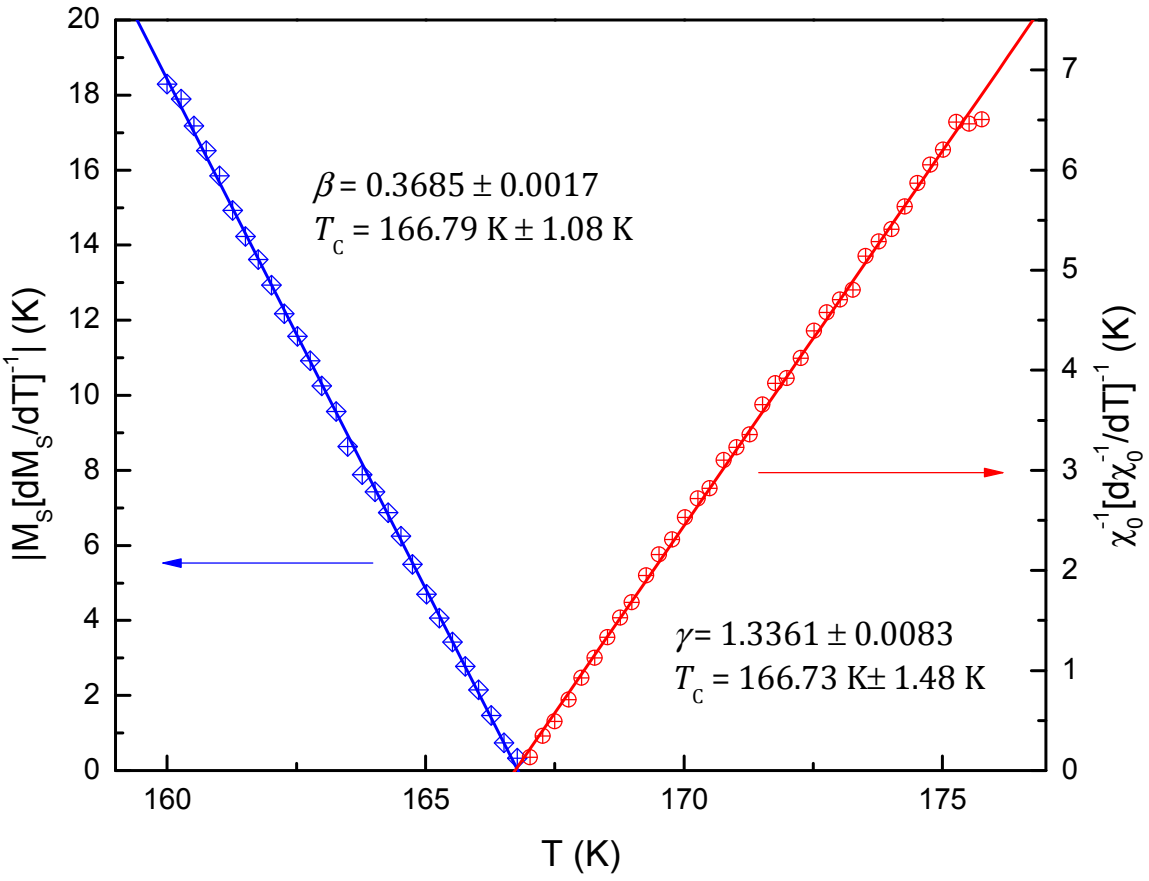
$\beta = 0.3685 \pm 0.0017$
$T_C = 166.79\ \text{K} \pm 1.08\ \text{K}$
$\gamma = 1.3361 \pm 0.0083$
$T_C = 166.73\ \text{K} \pm 1.48\ \text{K}$
$|M_S[dM_S/dT]^{-1}|$ (K)
$\chi_0^{-1}[d\chi_0^{-1}/dT]^{-1}$ (K)
T (K)
0
2
4
6
8
10
12
14
16
18
20
1
3
5
7
160
165
170
175

Fig. 6

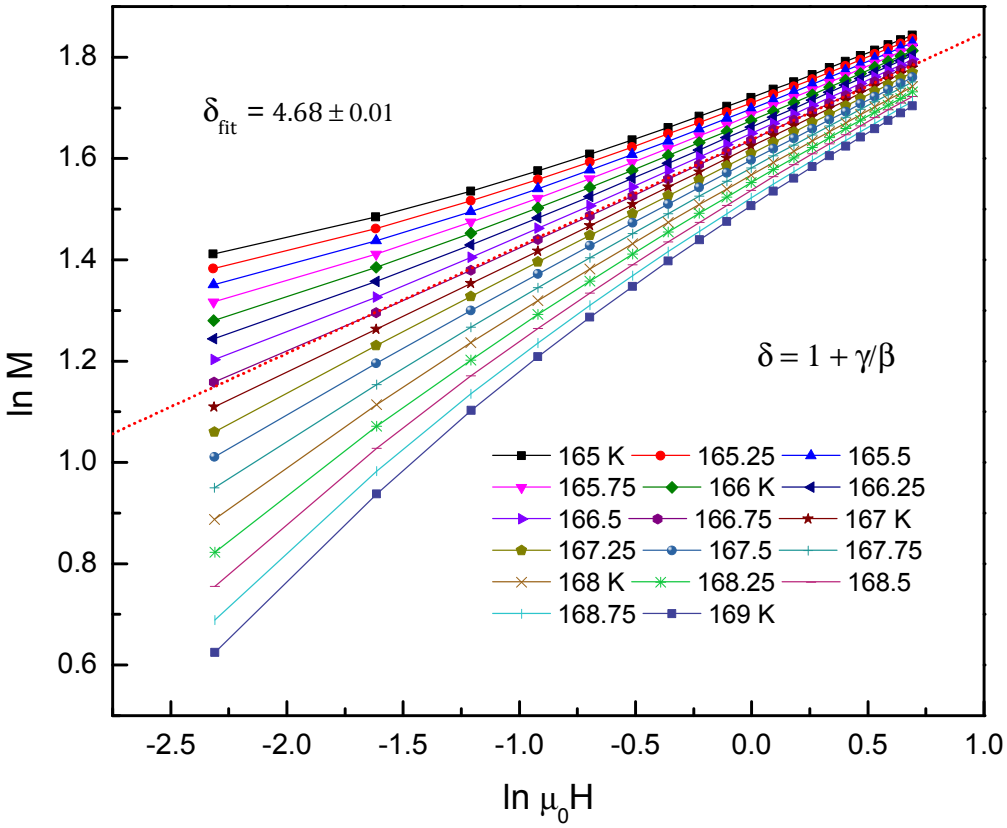
δfit = 4.68 ± 0.01
δ = 1 + γ/β
ln M
ln μ0H
1.8
1.6
1.4
1.2
1.0
0.8
0.6
-2.5
-2.0
-1.5
-1.0
-0.5
0.0
0.5
1.0
165 K
165.25
165.5
165.75
166 K
166.25
166.5
166.75
167 K
167.25
167.5
167.75
168 K
168.25
168.5
168.75
169 K

Fig. 7

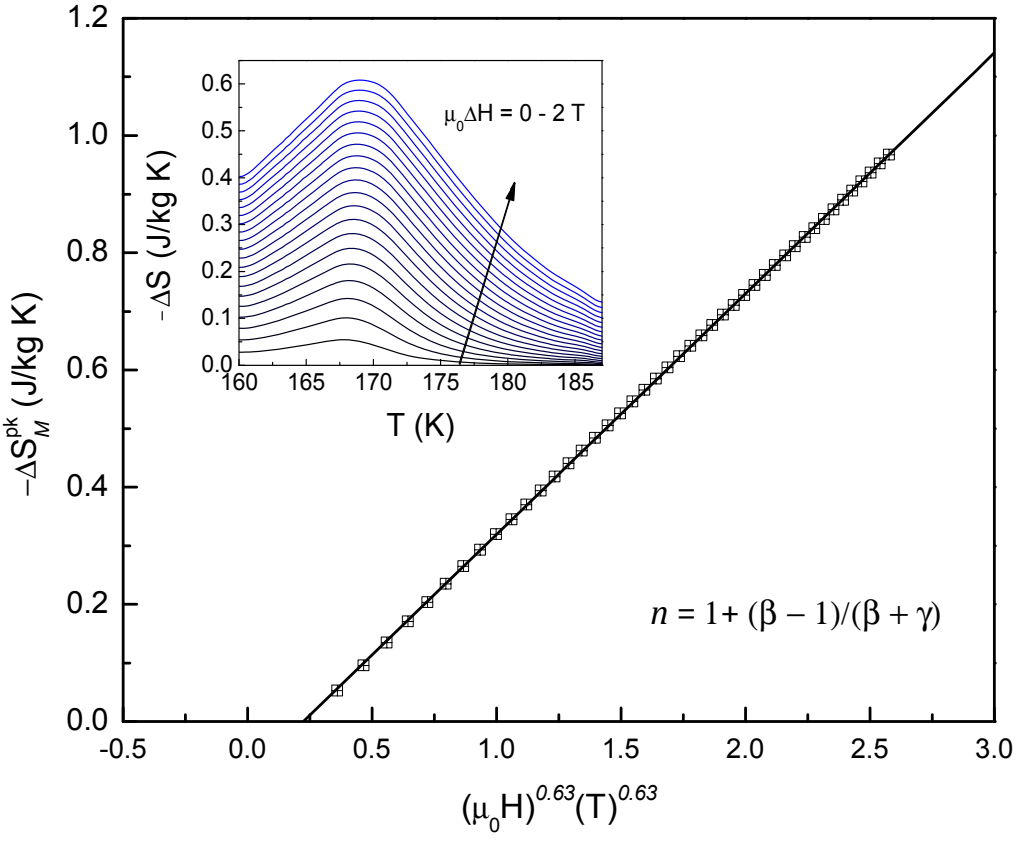
1.2
1.0
0.8
0.6
0.4
0.2
0.0
-0.5
0.0
0.5
1.0
1.5
2.0
2.5
3.0
$-\Delta S_M^{pk}$ (J/kg K)
$(\mu_0 H)^{0.63}(T)^{0.63}$
$n = 1 + (\beta - 1)/(\beta + \gamma)$
$-\Delta S$ (J/kg K)
T (K)
$\mu_0 \Delta H$ = 0 - 2 T
0.6
0.5
0.4
0.3
0.2
0.1
0.0
160
165
170
175
180
185

Fig. 8

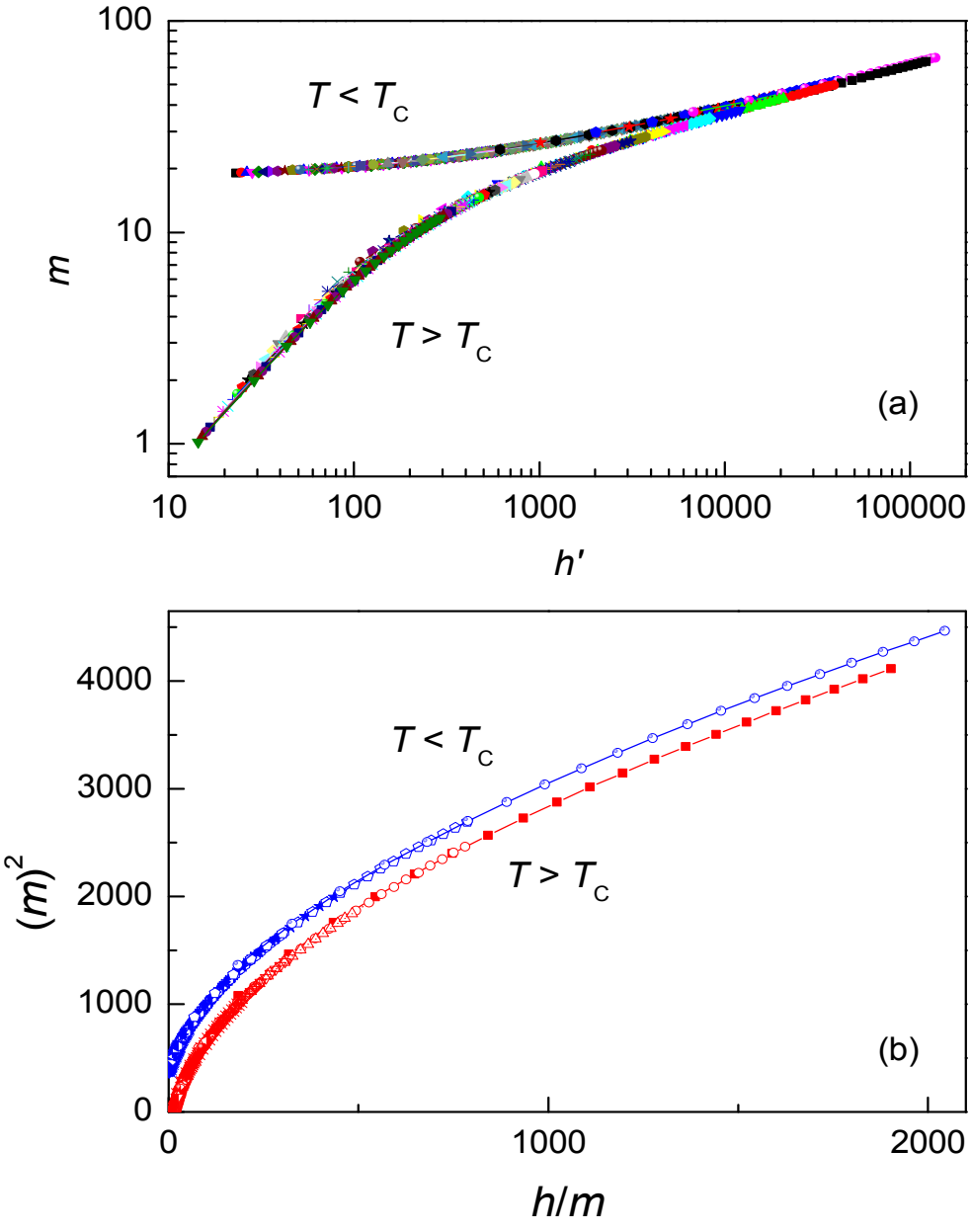
100
10
1
m
T < T_C
T > T_C
(a)
10
100
1000
10000
100000
h'
4000
3000
2000
1000
0
(m)^2
T < T_C
T > T_C
(b)
0
1000
2000
h/m

Fig. 9

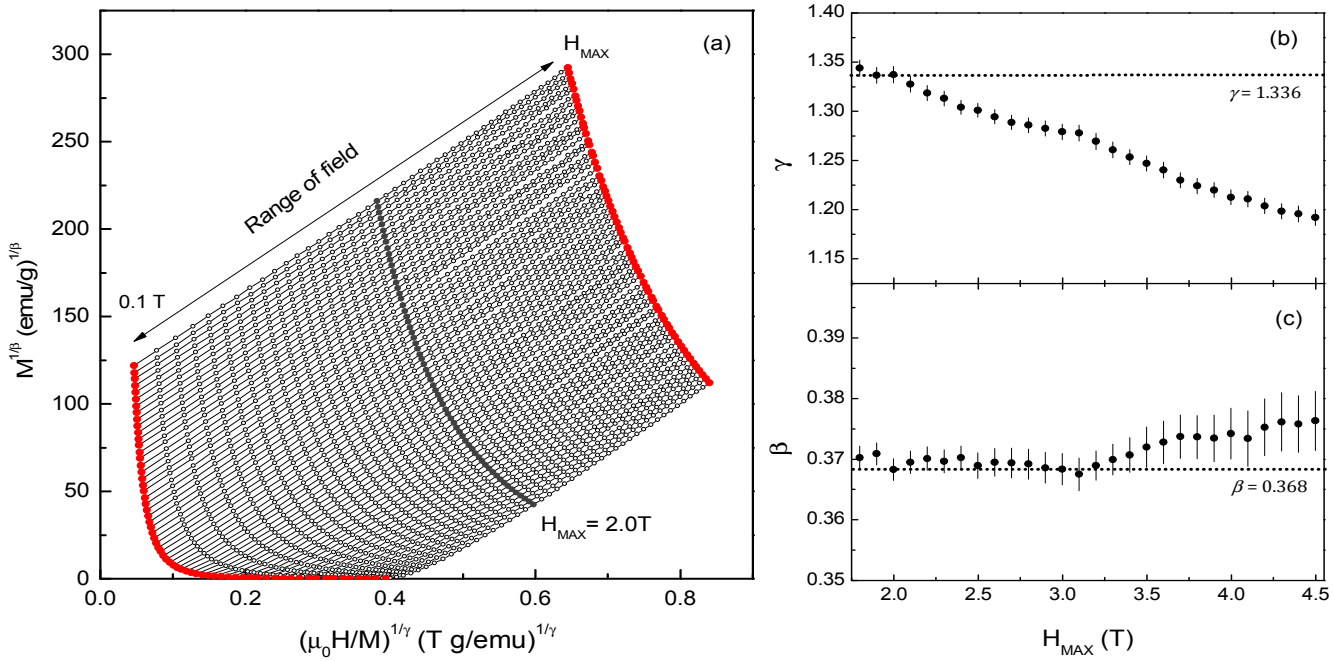
(a)
H_MAX
Range of field
0.1 T
H_MAX= 2.0T
M^1/β (emu/g)^1/β
(μ0H/M)^1/γ (T g/emu)^1/γ
(b)
γ= 1.336
γ
(c)
β = 0.368
β
H_MAX (T)

Fig. 10

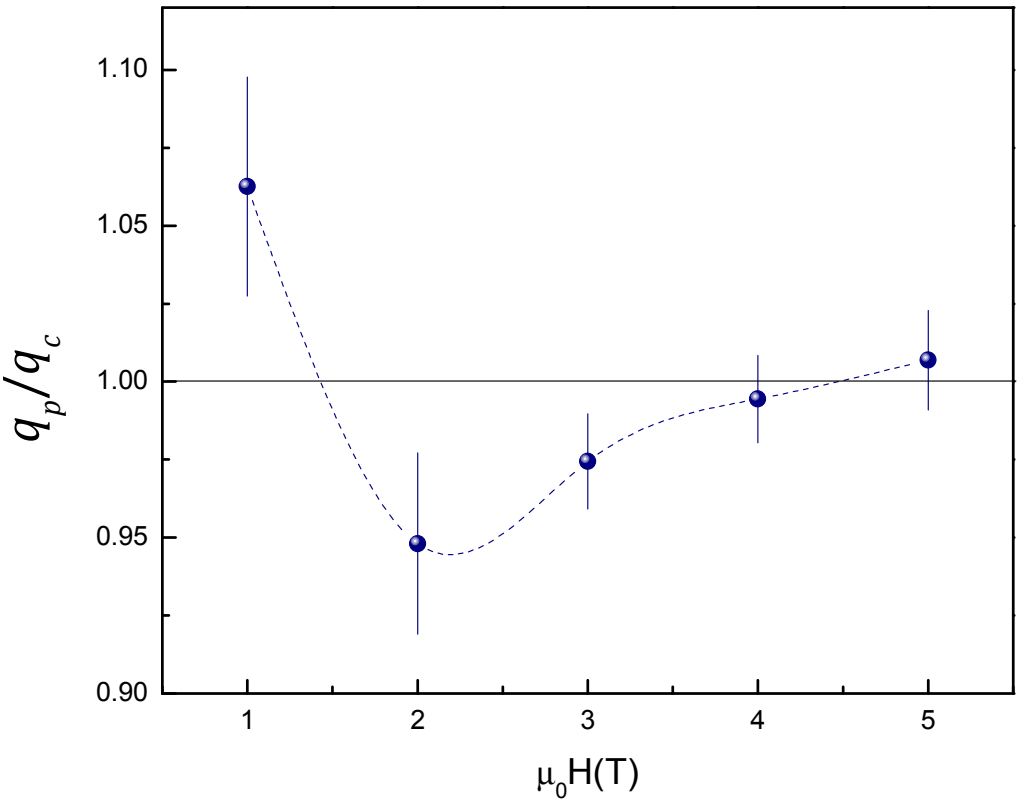

Fig. 11

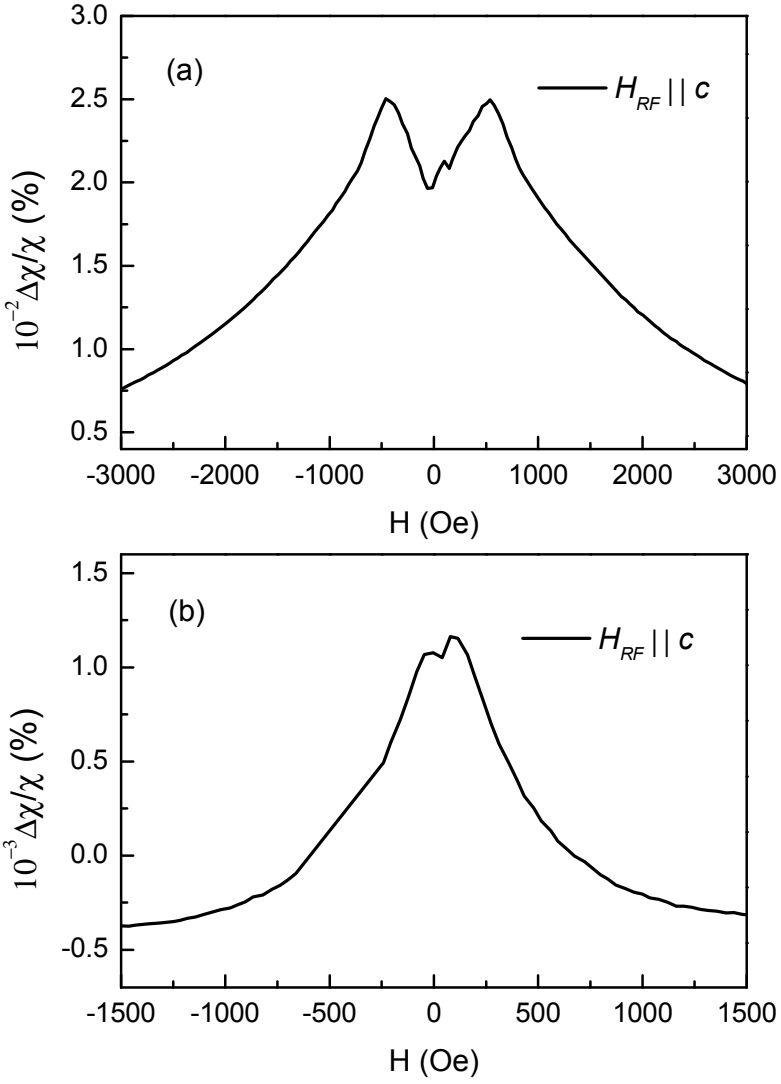
(a)
H_{RF} || c
$10^{-2}\Delta\chi/\chi$ (%)
3.0
2.5
2.0
1.5
1.0
0.5
-3000
-2000
-1000
0
1000
2000
3000
H (Oe)
(b)
H_{RF} || c
$10^{-3}\Delta\chi/\chi$ (%)
1.5
1.0
0.5
0.0
-0.5
-1500
-1000
-500
0
500
1000
1500
H (Oe)